

Saturation of Spin-Polarized Current in Nanometer Scale Aluminum Grains

Y. G. Wei, C. E. Malec, D. Davidović

School of Physics, Georgia Institute of Technology, Atlanta, GA 30332

(Dated: October 21, 2018)

We describe measurements of spin-polarized tunnelling via discrete energy levels of single Aluminum grains. In high resistance samples ($\sim G\Omega$), the spin-polarized tunnelling current rapidly saturates as a function of the bias voltage. This indicates that spin-polarized current is carried only via the ground state and the few lowest in energy excited states of the grain. At the saturation voltage, the spin-relaxation rate T_1^{-1} of the highest excited states is comparable to the electron tunnelling rate: $T_1^{-1} \approx 1.5 \cdot 10^6 s^{-1}$ and $10^7 s^{-1}$ in two samples. The ratio of T_1^{-1} to the electron-phonon relaxation rate is in agreement with the Elliot-Yafet scaling, an evidence that spin-relaxation in Al grains is governed by the spin-orbit interaction.

INTRODUCTION

Electron tunnelling through single nanometer scale metallic grains at low temperatures can display a discrete energy level spectrum. [1] Tunnelling spectroscopy of the energy spectra have led to numerous discoveries, including Fermi-Liquid coupling constants between quasiparticles, [2] spin-orbit interactions, [3, 4] and superconducting correlations in zero-dimensional systems. [5] Some information regarding the spin of an electron occupying a discrete level can be obtained using spin-unpolarized tunnelling, such as spin-multiplicity and electron g-factors. [1]

In this letter we report on spin-polarized tunnelling via discrete energy levels of single aluminum grains. Spin-polarized electron transport permits studies of spin relaxation and spin dephasing. [6, 7] By comparison, spin-unpolarized spectroscopy is suitable for the studies of energy relaxation in the grains. [1, 2] Since spin-relaxation times are generally many orders of magnitude longer than energy relaxation times, spin-unpolarized spectroscopy is not an easy tool to study spin-relaxation in the grains and spin-polarized tunnelling is needed. We find that some electron spin-relaxation times in Al grains are exceptionally long compared to bulk Al with similar disorder, on the order of μs .

Spin-polarized transport via metallic grains has recently generated a lot of theoretical interest. [8, 9, 10, 11, 12] In addition, there is a major effort to study nanospintronics using carbon-nanotubes; see Ref. [13] and references therein. Spin-coherent electron tunnelling via nanometer scale normal metallic grains has been confirmed in arrays [14, 15] and in single grains. [16] However, the electron spin-relaxation time T_1 in a metallic grain has not been reported yet.

SAMPLE FABRICATION

Our samples are prepared by electron beam lithography and shadow evaporation, similar to the technique described previously. [3] First we define a resist bridge

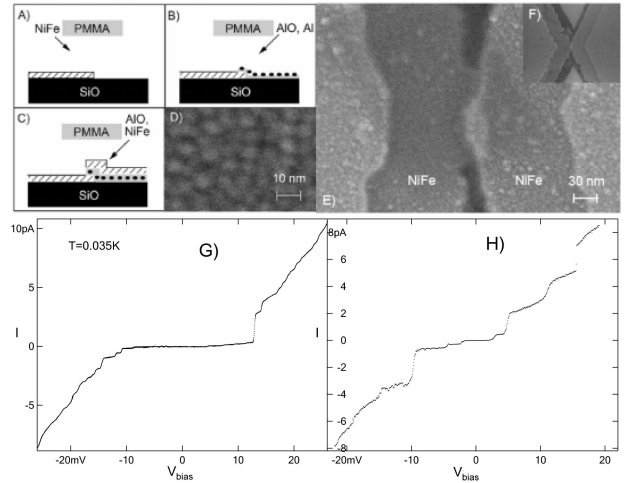


FIG. 1: A, B, C: Sample fabrication steps. D: Image of Al grains. E, F: Image of a typical sample. G, H: I-V curves at the base temperature.

placed 250 nm above the Si wafer; this bridge acts as a mask. Next (Fig. 1-A), we deposit 11 nm permalloy ($Py = Ni_{0.8}Fe_{0.2}$) onto oxidized silicon substrate at $4 \cdot 10^{-7}$ Torr base pressure, measured near the gate valve, along the direction indicated by the arrow. Then we rotate the sample by 36 degrees without breaking the vacuum and deposit 1.2 nm of Al_2O_3 by reactive evaporation of Al, [3] at a rate of 0.35 nm/s, at an oxygen pressure of $2.5 \cdot 10^{-5}$ Torr. Now, oxygen flow is shut down. When pressure decreases to the 10^{-7} Torr range, we deposit a 0.6 nm thick film of Al, as shown in Fig. 1-B. Al forms isolated grains with a typical diameter of 5 nm. The grains are displayed by the scanning electron microscope (SEM) image in Fig. 1-D. Finally we deposit another 1.2 nm layer of Al_2O_3 by the reactive evaporation and top it of by an 11 nm thick film of Py (Fig. 1-C). We make many samples on the same silicon wafer, and vary the overlap from 0 to 50 nm and select the devices with the highest resistance, as they have the smallest overlap. Figs. 1-E and F show SEM images of a typical device.

DISCRETE ENERGY LEVELS

Transport properties of the samples at low temperatures were measured using an Ithaco current amplifier. The samples were cooled down to $\approx 0.035K$ base temperature. The sample leads were cryogenically filtered to reduce the electron temperature down to $\approx 0.1K$.

The majority of samples (>80%) exhibit Coulomb Blockade at low temperature. About 150 samples were measured at 4.2K and 16 samples at 0.035K. In this paper we describe two samples. The I-V curve of two samples are shown in Fig. 1-G and H. The tunnelling current increases in discrete steps as a function of bias voltage, corresponding to discrete electron-in-a-box energy levels of the grain.

In sample 1, the average electron-in-a-box level spacing caused by electron geometric confinement is $\delta \approx 0.8meV$, which corresponds to diameter of $D \approx 6nm$ assuming a spherical Al grain. The average current step is $\bar{I} \approx 0.47pA$. We make a connection with the tunnelling rates from the leads to the grain and the measured current response. The tunnel junctions are highly asymmetric, and therefore one of the tunnelling rates is much smaller than the other, and thus rate limiting. Throughout this paper, we choose the rate limiting step to be across the left junction, corresponding to the tunnelling rate Γ_L . Therefore, our measured current corresponds to the average tunnelling-in rate of $\bar{\Gamma}_L = \bar{I}/2|e| \approx 1.5 \cdot 10^6 s^{-1}$. Similarly, in sample 2, $\delta \approx 2.7meV$, $D \approx 4nm$, and $\bar{\Gamma}_L \approx 9.6 \cdot 10^6 s^{-1}$.

The spin-conserving energy-relaxation in Al grains takes place by phonon emission with the relaxation rate [2]

$$\tau_{e-ph}^{-1}(\omega) = \left(\frac{2}{3}E_F\right)^2 \frac{\omega^3 \tau_e \delta}{2\rho \hbar^5 v_s^5}, \quad (1)$$

where $E_F = 11.7eV$ is the Fermi energy, ω is the energy difference between the initial and the final state, $\rho = 2.7g/cm^3$ is the ion-mass density, and $v_s = 6420m/s$ is the sound velocity. We obtain $\tau_{e-ph}^{-1}(\delta) \approx 1.6 \cdot 10^9 s^{-1}$ and $4.1 \cdot 10^{10} s^{-1}$ in samples 1 and 2, respectively. Sample 2 has significantly larger relaxation rate because of the larger level spacing. Since the tunnelling rates in our samples are $\sim 10^6 s^{-1}$, if the grain is excited by electron tunnelling in and out, it will instantly relax to the lowest energy state accessible by spin-conserving transitions.

As shown by Fig. 2, the energy levels exhibit Zeeman splitting as a function of an applied magnetic field. In sample 1, the I-V curve probes the same energy spectrum at negative and positive bias voltage. This is evident from the equivalence of the magnetic field dependencies at negative and positive bias. The lowest tunnelling threshold is two fold degenerate at zero magnetic field, showing that N_0 , the number of electrons on the grain before tunnelling in, is even. The conductance peaks are

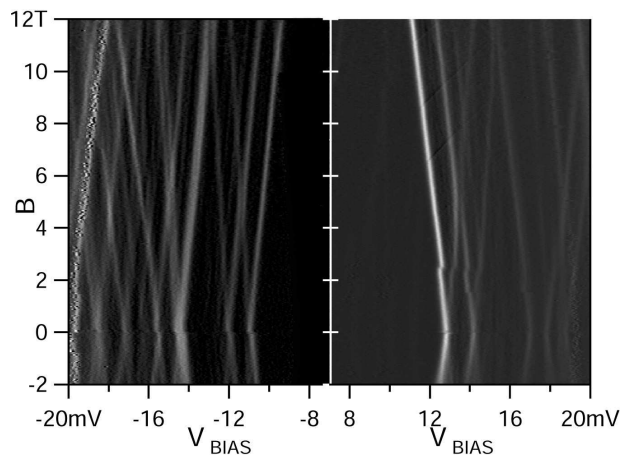


FIG. 2: A, B: Differential conductance (gray) versus bias voltage and the applied magnetic field in sample 1 at the base temperature.

similar in magnitude at negative bias, because the first tunnelling step, in which an electron tunnels in to the grain through the higher resistance junction, is rate limiting. At positive bias, the first conductance peak is much larger than the subsequent conductance peaks, because the first tunnelling step takes place via the lower resistance junction, and the rates are limited by the electron discharge process across the high resistance junction.

In sample 1, the first two peaks split corresponding to g-factors: $g = 1.83 \pm 0.05$ and 1.95 ± 0.05 . Slight reduction of the g-factors from 2 indicates spin-orbit interaction in Al. [1] The avoided level crossings clearly are resolved in Fig. 2, near points $(-11.5mV, 5T)$ and $(-13mV, 11.5T)$. The corresponding avoided crossings at positive bias are located near $(13.5mV, 5T)$ and $(15.5mV, 11.5T)$, respectively. In the regime where g factors are slightly reduced, the spin-orbit scattering rate (τ_{SO}^{-1}) can be obtained from the avoided crossing energies $\Delta_{SO} \approx 0.1meV$. [17] Theory predicts that $\tau_{SO} \approx \hbar\delta/\pi\Delta_{SO}^2$, [17] within a factor of two. Thus, we obtain $\tau_{SO}^{-1} \approx 5.5 \cdot 10^{10} s^{-1}$. By the Elliot-Yafet relation, [18] τ_{SO}^{-1} is related to the elastic scattering rate τ_e^{-1} : $\tau_{SO}^{-1} = \alpha\tau_e^{-1}$. Assuming ballistic grain, $\tau_e^{-1} \approx v_F/D = 3.4 \cdot 10^{14} sec^{-1}$. We obtain $\alpha \approx 1.6 \cdot 10^{-4}$, in excellent agreement with $\alpha \approx 10^{-4}$ in Al thin films. [19]

SPIN-POLARIZED TUNNELLING

Now we discuss magnetoresistance from the spin-polarized tunnelling. In the magnetic field range of $\pm 50mT$, approximately 90% of the samples do not display any of the tunnelling magnetoresistance effect (TMR). By contrast, we tested about 10 tunnelling junctions without the embedded grains and with similar resistance (empty junctions) at 4.2 K. All of the empty

junctions exhibit a significant TMR in this field range, comparable to 10%. Approximately one half of the empty junctions display a simple spin-valve effect. So, the absence of TMR for electron tunnelling via grains shows that the spin-dephasing rate T_2^{-1} in 90% of the samples must be much larger than the tunnelling rate.

Nevertheless, approximately 10% of the samples with embedded grains display significant TMR, so the dephasing must be weak, e.g. T_2^{-1} must be smaller than or comparable to the tunnelling rate in these samples. T_2 variation among different samples could be explained by magnetic defects, such as paramagnetic impurities from the Py layer. Paramagnetic impurities are common sources of dephasing. [20] The defects would be located on the grain surface, since bulk Al does not support paramagnetism. Since the number of atoms on the surface is relatively small (~ 1000), we could occasionally obtain a sample free of impurities. More insight into the nature of T_2 in this device will require a more in depth theoretical study.

A majority of the samples with nonzero TMR show positive TMR near the Coulomb-Blockade conduction threshold; only about 30% of the samples show negative TMR. The sign of TMR in quantum dots is determined by the interplay between charging effects and spin-accumulation. [15, 21] For any given sample, the data in this paper correspond to the voltage range within the first step of the Coulomb staircase. In this range the sign of TMR is found to be constant as expected.

TMR in our devices usually does not display a simple spin-valve effect. We believe this is because there are spin-dependent interactions inside the grain that induce a complicated TMR even when the magnetic transitions in the drain and source leads are sharp and as expected. For example, a rotation of stray magnetic field acting on the grain will alter the direction of the spin-quantization axis in the grain, thereby changing the conductance [8]. A rotation or a switch of a remote domain can change the tunnelling current through the grain via the magnetic field generated by the domain. Similarly, the orientation of the nuclear spin in the grain can change the quantization axes via the hyperfine interaction.

We select only those samples that display a simple spin-valve TMR effect, which is shown in Figs. 3. Fig. 3-A is the TMR of sample 1 at a bias voltage corresponding to the second current plateau. TMR is barely resolved in this case, since the current changes by only about 40fA. We do not have good data to display TMR at the first current plateau. By comparison, Figs. 3-B and C display TMR at bias voltage where the number of electron-in-a-box levels energetically available for tunnelling-in are approximately 19 and 48, respectively. To facilitate comparisons, the current intervals on the vertical axes in Figs. 3 A-C and D-F have equal lengths.

The main observation in this letter is that $\Delta I = I_{\uparrow\uparrow} - I_{\uparrow\downarrow}$ is nearly constant with current above a cer-

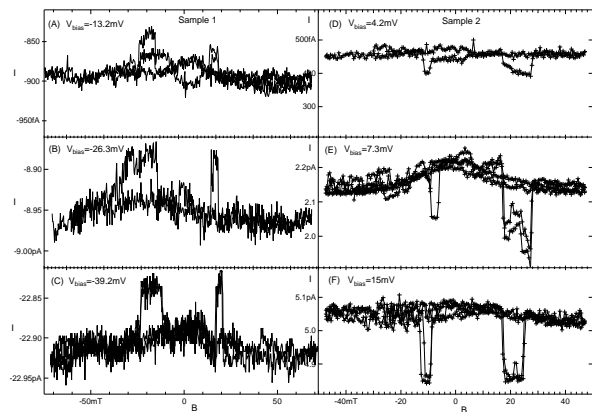


FIG. 3: A-F: Spin-valve effect in current versus applied magnetic field in two samples at the base temperature. The current magnitude is reduced in the antiparallel state.

tain current. There is hardly any increase in ΔI between Figs. 3 B and C and between Figs. 3 E and F. This behavior is shown in more detail Fig. 4-A and B, which displays ΔI versus bias voltage. ΔI versus negative bias voltage in sample 1 is fully saturated at the third current plateau; at the second current plateau, ΔI is already at one half of the saturation value. Similarly, in sample 2 ΔI reaches saturation at the second current plateau. Our samples should be contrasted with ordinary ferromagnetic tunnelling junctions, where ΔI is proportional to the current over a significantly wider range of bias voltage [22, 23].

INTERPRETATION OF THE RESULTS

In coulomb-blockade samples containing magnetic leads, the electrochemical potential difference between the island and leads can jump when the magnetization in one of the leads changes direction [10]. This can lead to a sudden shift in energy levels, producing a jump in current that is constant as a function of bias voltage. The shift in energy levels is seen as a discontinuity near zero magnetic field in Fig. 2, and is $\sim 0.1mV$.

To show that the electrochemical shift is not responsible for the saturation of the spin-polarized current with voltage in our sample, we performed other measurements by sweeping the magnetic field both on and between the current plateaus, coming up with similar values for the electrochemical shift. The shift is lower than the average level spacing of 0.8 meV and 2.7 meV for sample 1 and sample 2 respectively. Therefore, since we measured magnetoresistance in the middle of the current plateau, the threshold voltage shift should not effect our measurements of the saturation in ΔI .

To explain $I_{\uparrow\uparrow} - I_{\uparrow\downarrow} = const$, we must discuss the relative magnitudes of three rates: τ_{e-ph}^{-1} , the rate of en-

ergy relaxation from excited to lower energy states by spin-conserving phonon emission; Γ_L , the rate electrons tunnel into the grain; and T_1^{-1} , the rate of transitions between levels that result in an electron flipping its spin orientation. τ_{e-ph}^{-1} is obtained theoretically, the measured I-V spectrum fixes the tunnelling rate, and T_1^{-1} is obtained from the saturation in $I_{\uparrow\uparrow} - I_{\uparrow\downarrow}$ with bias voltage.

Finally we must deduce the relative magnitude of T_1^{-1} . The rate of spin-flip transitions is expected to be significantly smaller than τ_{e-ph}^{-1} [18]. In this case the ground state would not necessarily be accessible by energy relaxation. The grain could remain in an excited, spin-polarized state, as sketched in Fig. 4-C. These spin-polarized excited states are responsible for spin accumulation in the antiparallel magnetic configuration of the leads. If the relaxation rates for the spin-flip transitions are much smaller than the tunnelling rate, then various spin-polarized states would have similar probabilities, which are determined by the tunnelling rates. In the antiparallel configuration of the leads, the probabilities of the excitations with spin up would be enhanced by $1 + P$ and probabilities of the excitations with spin down would be suppressed by $1 - P$, where P is the spin-polarization in the leads. In the parallel configurations, the probabilities of the excitations with spin up and spin down are the same. In this regime, $I_{\uparrow\uparrow} - I_{\uparrow\downarrow}$ is proportional to the current, similar to the usual ferromagnetic tunnelling junctions.

It is reasonable to expect that the spin-flip rate $T_1^{-1}(\omega)$ increases rapidly with energy difference ω between the initial and the final state [24]. If $T_1^{-1}(\omega)$ exceeds the tunnelling rate above some ω , then the excitations with energy $> \omega$ will occur with a reduced probability in the ensemble of states generated by tunnelling in and out. Thus ΔI is limited by tunnelling via the ground state and those low lying spin-polarized states where $T_1^{-1}(\omega) < \Gamma_L$. ΔI versus bias voltage approaches saturation approximately when $T_1^{-1}(\omega) = \Gamma_L$, where ω is the highest excitation energy in the ensemble of spin-polarized states generated by tunnelling in and out: $\omega \approx \delta \frac{1}{e\Gamma_L}$. This is how we determine the spin-relaxation time $T_1(\omega)$ at an energy ω in a given sample.

In sample 1, ΔI is at 50% of the saturation value at the second current plateau, and ΔI is saturated at the third current plateau. At the second current plateau, the spin-relaxation rate of the highest energy excited state generated by tunnelling must be close to the tunnelling rate. Since the spin relaxation is very rapid in configurations more than 3δ above the ground state, and N_0 is even as noted above, the grain spends most of the time among the five configurations shown in Fig. 4-C: N_0 , N_0^+ , N_0^- , N_0^{++} , and N_0^{--} . The highest energy spin-polarized states are N_0^{++} and N_0^{--} . Thus, $T_1^{-1}(3\delta) \approx \Gamma_L = 1.5 \cdot 10^6 s^{-1}$. In sample 2, this analysis leads to $T_1^{-1}(2\delta) \approx 10^7 s^{-1}$.

Now we discuss the origin of spin relaxation and its

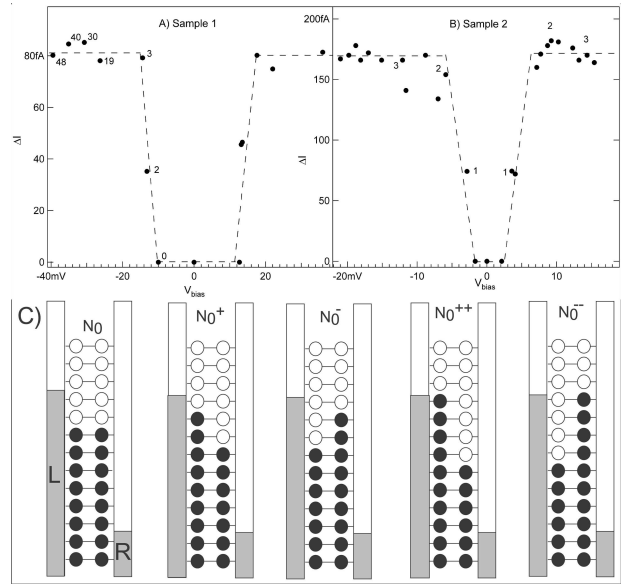


FIG. 4: A and B: $\Delta I = |I_{\uparrow\uparrow} - I_{\uparrow\downarrow}|$ versus bias voltage in samples 1 and 2, respectively, at the base temperature. The numbers near the circles indicate how many doubly degenerate electron-in-a-box levels are available for tunnelling in. C: Possible spin-polarized electron configurations caused by electron tunnelling in and out, before an electron tunnels in, at the second current plateau, for N_0 even.

rapid enhancement with the energy difference. Note that the rate of spin-conserving transitions in Eq. 1 increases as ω^3 . We suggest that the electron-phonon transition rates without and with spin flip scale by the Elliot-Yafet relation: $T_1^{-1}(\omega) = \alpha' \tau_{e-ph}^{-1}(\omega)$. This scaling would certainly explain the rapid increase in spin-relaxation rate with excitation energy. In metallic films, it is well established that the Elliot-Yafet scaling applies for both elastic and inelastic scattering processes, with $\alpha \approx \alpha'$. [19]

In sample 1, Eq. 1 leads to $\tau_{e-ph}^{-1}(3\delta) \approx 4 \cdot 10^{10} s^{-1}$. Since $T_1^{-1}(3\delta) \approx 1.5 \cdot 10^6 s^{-1}$, we obtain $\alpha' \approx 0.4 \cdot 10^{-4}$. Similarly, in sample 2, $\tau_{e-ph}^{-1}(2\delta) \approx 3.3 \cdot 10^{11} s^{-1}$ and we obtain $\alpha' \approx 0.3 \cdot 10^{-4}$. α' agrees with $\alpha \approx 1.5 \cdot 10^{-4}$ obtained earlier, within an order of magnitude. So the ratio of τ_{e-ph} and T_1 is in agreement with the Elliot-Yafet scaling. This is an evidence that the spin-flip transitions in Al grains are driven by the spin-orbit interaction. By this relaxation mechanism, the spin of an electron on the grain is coupled to the phonon continuum via the spin-orbit interaction. An electron in an excited spin-polarized state relaxes by an emission of a phonon, which has an angular momentum equal to the difference between the initial and final electron spin.

CONCLUSION

In summary, we have observed spin-coherent electron transport via discrete energy levels of single Al grains. Spin polarized current saturates quickly as a function of bias voltage, which demonstrates that the ground state and the lowest excited states carry spin polarized current. Higher excited states have a relaxation time shorter than the tunnelling time and they do not carry spin-polarized current. The spin-relaxation time of the low-lying excited states is $T_1 \approx 0.7\mu s$ and $0.1\mu s$ in two samples. Finally, the ratio of the spin-flip transition rate and the electron-phonon relaxation rate is in quantitative agreement with the Elliot-Yafet scaling ratio, an evidence that the spin-relaxation transitions are driven by the spin-orbit interaction.

This work was performed in part at the Georgia-Tech electron microscopy facility. We thank Matthias Braun and Markus Kindermann for consultation. This research is supported by the DOE grant DE-FG02-06ER46281 and David and Lucile Packard Foundation grant 2000-13874.

-
- [1] D. C. Ralph, C. T. Black, and M. Tinkham, *Phys. Rev. Lett.* **74**, 3241 (1995).
 - [2] O. Agam, N. S. Wingreen, B. L. Altshuler, D. C. Ralph, and M. Tinkham, *Phys. Rev. Lett.* **78**, 1956 (1997).
 - [3] D. Davidović and M. Tinkham, *Phys. Rev. Lett.* **83**, 1644 (1999).
 - [4] J. R. Petta and D. C. Ralph, *Phys. Rev. Lett.* **87**, 266801 (2001).
 - [5] C. T. Black, D. C. Ralph, and M. Tinkham, *Phys. Rev. Lett.* **76**, 688 (1996).
 - [6] M. Johnson and R. H. Silsbee, *Phys. Rev. Lett.* **55**, 1790 (1985).
 - [7] F. J. Jedema, H. B. Heersche, A. T. Filip, J. J. A. Baselmans, and B. J. van Wees, *Nature* **416**, 713 (2002).
 - [8] M. Braun, J. König, and J. Martinek, *Europhys. Lett.* **72**, 294 (2005).
 - [9] I. Weymann and J. Barnas, *Phys. Rev. B* **73**, 205309 (2006).
 - [10] S. J. van der Molen, N. Tombros, and B. J. van Wees, *Phys. Rev. B* **73**, 220406(R) (2006).
 - [11] W. Wetzels, G. E. W. Bauer, and M. Grifoni, *Phys. Rev. B* **74**, 224406 (2006).
 - [12] A. Cottet and M. S. Choi, *Phys. Rev. B* **74**, 235316 (2006).
 - [13] A. Cottet, T. Kontos, S. Sahoo, H. T. Man, M. S. Choi, W. Belzig, C. Bruder, A. F. Morpurgo, and C. Schonenberger, *Semicon. Sci. and Tech.* **21**, S78 (2006).
 - [14] L. Zhang, C. Wang, Y. Wei, X. Liu, and D. Davidović, *Phys. Rev. B* **72**, 155445 (2005).
 - [15] F. Ernult, K. Yakushiji, S. Mitani, and K. Takanaishi, *J. Phys. Cond. Mat.* **19**, 1652140 (2007).
 - [16] A. Bernard-Mantel, P. Seneor, N. Lidgi, M. Munoz, V. Cros, S. Fusil, K. Bouzehouane, C. Deranlot, A. Vares, F. Petroff, et al., *Appl. Phys. Lett.* **89**, 062502 (2006).
 - [17] S. Adam, M. L. Polianski, X. Waintal, and P. W. Brouwer, *Phys. Rev. B* **66**, 195412 (2002).
 - [18] Y. Yafet, *Sol. State Phys.* **14**, 1 (1963).
 - [19] F. J. Jedema, M. S. Nijboer, A. T. Filip, and B. J. van Wees, *Phys. Rev. B* **67**, 085319 (2003).
 - [20] G. Bergman, *Phys. Rep.* **107**, 1 (1984).
 - [21] J. Barnas and A. Fert, *Phys. Rev. Lett.* **80**, 1058 (1998).
 - [22] J. S. Moodera, J. Nowak, and R. J. M. van de Veerdonk, *Phys. Rev. Lett.* **80**, 2941 (1998).
 - [23] S. Zhang, P. M. Levy, A. C. Marley, and S. S. P. Parkin, *Phys. Rev. Lett.* **79**, 3744 (1997).
 - [24] In bulk metals the spin-orbit scattering rate increases rapidly with electron excitation energy